2012

Design optimization and comparative analysis of silicon-nanowire-based couplers

Hongqiang Li
Tianjin Polytechnic University, lihongqiang@tjpu.edu.cn

Xiaye Dong
Tianjin Polytechnic University

Enbang Li
University of Sydney, enbang@uow.edu.au

Zhihui Liu
Tianjin Polytechnic University, 88girllzh@sina.com

Yaoting Bai
Tianjin Polytechnic University

Publication Details

Li, H., Dong, X., Li, E., Liu, Z. & Bai, Y. (2012). Design optimization and comparative analysis of silicon-nanowire-based couplers. IEEE Photonics Journal, 4 (5), 2017-2026.

Design optimization and comparative analysis of silicon-nanowire-based couplers

Abstract
Three kinds of highly compact 2 x 2 couplers based on silicon nanowire are designed and optimized for the array waveguide grating (AWG) demodulation integration microsystem in this paper. These couplers are directional (X) coupler, cross gap coupler (CGC), and multimode interface (MMI) coupler. The couplers are simulated using the beam propagation method. The distance between the input/output waveguides is set to 10 μm considering the test of a single device in the following work. The total footprint of X coupler is 10 μmx 300 μm. The length of parallel film waveguide is 1 μm. After optimization, the minimum excess loss is 0.73 dB. CGC has a footprint of 10 μm x 300 μm , a coupling region length of 24 μm, and a minimum excess loss of 0.6 dB. Taper waveguides are used as input/output waveguides for MMI coupler. The footprint of MMI region is only 6 μm x 57 μm. The excess loss is 0.46 dB after optimization. Uniformity is 0.06 dB with transverse electric polarization when the center wavelength is 1.55 μm. The maximum excess loss is 1.55 dB in the range of 1.49 μm to 1.59 μm. The simulation results show that a small 2 x 2 MMI coupler exhibits lower excess loss, wider bandwidth, and better uniformity than X coupler and CGC. MMI coupler is suitable for the requirements of optoelectronic integration. 2012 IEEE.

Keywords
nanowire, silicon, analysis, couplers, comparative, design, optimization

Publication Details
Li, H., Dong, X., Li, E., Liu, Z. & Bai, Y. (2012). Design optimization and comparative analysis of silicon-nanowire-based couplers. IEEE Photonics Journal, 4 (5), 2017-2026.

IEEE Photonics Journal
An IEEE Photonics Society Publication

Open Access

Design Optimization and Comparative Analysis of Silicon-Nanowire-Based Couplers

Volume 4, Number 5, October 2012

Hongqiang Li
Xiaye Dong
Enbang Li
Zhihui Liu
Yaoting Bai

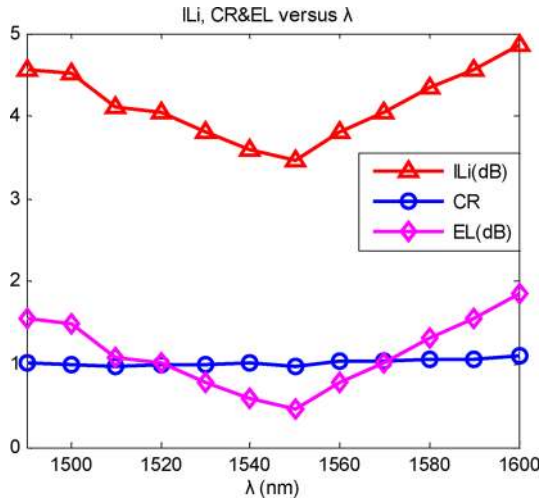

DOI: 10.1109/JPHOT.2012.2222364
1943-0655/$31.00 ©2012 IEEE

Design Optimization and Comparative Analysis of Silicon-Nanowire-Based Couplers

Hongqiang Li,[1] Xiaye Dong,[1] Enbang Li,[2] Zhihui Liu,[1] and Yaoting Bai[1]

[1]School of Electronics and Information Engineering, Tianjin Polytechnic University, Tianjin 300387, China
[2]Centre for Ultrahigh bandwidth Devices for Optical Systems (CUDOS), The University of Sydney, New South Wales 2006, Australia

DOI: 10.1109/JPHOT.2012.2222364

Manuscript received September 9, 2012; revised September 28, 2012; accepted September 28, 2012. Date of publication October 5, 2012; Date of current version October 18, 2012. This work was supported in part by the National Natural Science Foundation of China under Grants 61177078 and 60877049 and in part by the Specialized Research Fund for the Doctoral Program of Higher Education of China under Grant 20101201120001. Corresponding author: H. Li (e-mail: lihongqiang@tjpu.edu.cn).

Abstract: Three kinds of highly compact 2 × 2 couplers based on silicon nanowire are designed and optimized for the array waveguide grating (AWG) demodulation integration microsystem in this paper. These couplers are directional (X) coupler, cross gap coupler (CGC), and multimode interface (MMI) coupler. The couplers are simulated using the beam propagation method. The distance between the input/output waveguides is set to 10 μm considering the test of a single device in the following work. The total footprint of X coupler is 10 μm × 300 μm. The length of parallel film waveguide is 1 μm. After optimization, the minimum excess loss is 0.73 dB. CGC has a footprint of 10 μm × 300 μm, a coupling region length of 24 μm, and a minimum excess loss of 0.6 dB. Taper waveguides are used as input/output waveguides for MMI coupler. The footprint of MMI region is only 6 μm × 57 μm. The excess loss is 0.46 dB after optimization. Uniformity is 0.06 dB with transverse electric polarization when the center wavelength is 1.55 μm. The maximum excess loss is 1.55 dB in the range of 1.49 μm to 1.59 μm. The simulation results show that a small 2 × 2 MMI coupler exhibits lower excess loss, wider bandwidth, and better uniformity than X coupler and CGC. MMI coupler is suitable for the requirements of optoelectronic integration.

Index Terms: Optical devices, silicon nanowire, coupler, loss, optoelectronic integration.

1. Introduction

An optical coupler is a passive optical device in the optical fiber grating demodulation system, with an irreplaceable and important function. Developing optical couplers with low cost, high performance, and high-level integration is urgent to meet the demodulation system requirements [1]. A directional (X) coupler, a two-mode-interference (TMI) coupler, a cross gap coupler (CGC), and a 2 × 2 multimode interference (MMI) coupler are designed and optimized in this paper. The X coupler depends greatly on the wavelength and has a large footprint, with a bandwidth of only about 10 nm. The TMI coupler and CGC have relatively smaller sizes and can be used as alternatives to X coupler. The TMI coupler and CGC depend greatly on the wavelength and are sensitive to polarization. MMI couplers have advantages such as compact construction, small size, simple fabrication techniques, large fabrication tolerance, low loss, and polarization insensitivity. Thus, MMI couplers are widely used in planar lightwave circuits [2], [3]. With the rapid development of integrated optics, MMI couplers have been applied in M–Z interferometer, optical switches, modulators, optical multiplexer–demultiplexer devices,

ring oscillators, and filters, among others [4], [5]. In recent years, researchers have worked on couplers based on silicon-on-insulator (SOI) to produce couplers with smaller size or lower excess loss [6], [7]. In 2008, Chen *et al.* introduced a femtosecond fiber laser applied to fabricate broadband X couplers inside bulk glass for general power splitting application in the 1250- to 1650-nm wavelength telecom spectrum [8]. In 2010, Tanaka *et al.* proposed and designed CGC based on SOI [9]. In 2012, Halir *et al.* designed a colorless X coupler with dispersion engineered subwavelength structure [10]. In 2006, Solehmainen *et al.* designed a 2×2 MMI coupler based on SOI with a multimode section footprint of 30.5 μm $\times$ 1394 μm and an excess loss of 0.5 dB [11]. In the same year, Xu *et al.* designed a 2×2 MMI coupler based on SOI with a multimode section footprint of 5 μm $\times$ 54 μm [12]. In 2011, Zhou *et al.* designed and fabricated 1×2 MMI couplers based on SOI with splitting ratios of 85 : 15 and 72 : 28 [13].

The aforementioned 2×2 couplers were applied in different optical devices. In this paper, the X couplers, CGC, and MMI couplers based on SOI are designed for the array waveguide grating (AWG) demodulation integration microsystem. The microsystem is a new kind of optical fiber grating demodulation scheme that is suitable for optoelectronic integration. The feature of our research subject is that the devices used in fiber grating demodulation system will be integrated on a single chip. It is a work that is different from Tanaka's. The couplers are used in the C-band because the light source for the fiber Bragg grating (FBG) demodulation system is usually in the C-band. The splitting ratio of the couplers should be 50:50 to obtain the maximum power for AWG. The couplers are simulated using the beam propagation method (BPM). This paper analyzes how the input/output waveguides affect the coupling length of X couplers. We also analyze how the multimode waveguide width affects the coupler properties [14], optimizes input/output waveguide to reduce loss, and analyzes coupler bandwidth [15]. Compared with previously designed couplers, the 2×2 couplers designed in this paper are highly compact, and MMI couplers exhibit low loss and wide bandwidth.

2. Design and Optimization of 2×2 Couplers

2.1. Designing Material

In this paper, SOI is selected as the material during simulation. SOI is a prominent platform for microelectronics and optoelectronics. As a material used in waveguide devices, SOI displays superiority in the following aspects: compatibility with silicon processing, convenient for electronic integration and photonic integration, waveguide characteristics, fast operation in optical circuit, and radio protection. SOI can be used in optical device interconnection and can be applied in military devices. Extremely small devices can be fabricated on SOI substrates because of the ultrahigh refractive index contrast between Si and SiO_2. Bent waveguides with smaller radius of curvature can be realized on SOI substrates. The refractive index contrast can be expressed as

$$\Delta = \frac{n_1 - n_2}{n_1} \times 100\% = 58.1\% \tag{1}$$

where n_1 is the refractive index of Si $(n_1 = 3.46)$, and n_2 is the refractive index of SiO_2 $(n_2 = 1.45)$.

2.2. Design and Optimization of Directional (X) Coupler

X coupler is based on the principle of power exchange between two waveguides approaching each other. The coupling region of X coupler is composed of two parallel film waveguides. The splitting ratio can be controlled by adjusting the coupling region length. The schematic of transverse coupling is shown in Fig. 1.

In weak coupling, the optical field of composite waveguides can be expressed as

$$\begin{cases} E_m = A_1(z)E_1 + A_2(z)E_2 \\ H_m = A_1(z)H_1 + A_2(z)H_2. \end{cases} \tag{2}$$

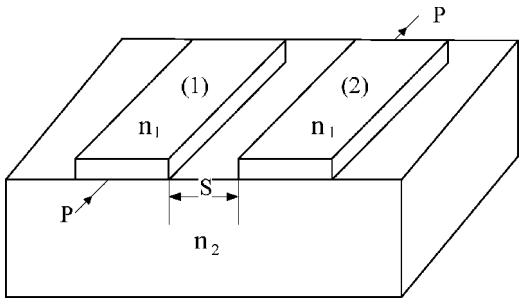

Fig. 1. Schematic illustration of transverse coupling.

The coupling length can be expressed as

$$L = \frac{\pi}{(n_e - n_o)k_0} \tag{3}$$

where n_e is the effective refraction index of the even symmetrical mode, n_o is the effective refraction index of the odd symmetrical mode, and k_0 is the vacuum vector. The coupling length for 3-dB X coupler is expressed as

$$L_{3dB} = \frac{L}{2} = \frac{\pi}{2(n_e - n_o)k_0}. \tag{4}$$

X coupler is simulated via BPM. The waveguide width is expressed as w. The distance between two parallel film waveguides is expressed as s. The optical field and output power of X coupler with different w and s are shown in Fig. 2.

The best simulation results of X coupler are shown in Fig. 2(e). The excess loss of the device is about 0.73 dB, and the footprint is 300 μm $\times$ 10 μm. The layout and detailed parameters of the coupler are shown in Fig. 3.

2.3. Design and Optimization of CGC

CGC is a coupler that has an X-junction with an internal cross-sectional mirror. The gap in CGC between two waveguides functions as a half-mirror. The principle of CGC is similar with X coupler. The difference between the two couplers is that the input/output waveguides of CGC are linear.

CGC is simulated via BPM in the present paper. The waveguide width is expressed as w. The gap is expressed as s. The optical field and output power of CGC with different w and s are shown in Fig. 4.

The best simulation results of CGC are shown in Fig. 4(e). The excess loss of the device is about 0.6 dB, and the footprint is 300 μm $\times$ 10 μm. The layout and detailed parameters of the coupler are shown in Fig. 5.

Table 1 shows the comparison of CGC and X coupler in Figs. 2 and 4. L stands for the input/output waveguide length, L_s stands for the coupling region length, and EL stands for the excess loss of the coupler.

As Fig. 2 and Fig. 4 show, the coupling region of X coupler exchanges energy periodically by coupling between the two parallel film waveguides. The output waveguides are set in the first period to reduce coupler length. The greater s is, the longer the coupling length. In the same w and s values, the coupling length of X coupler is relatively short, compared with CGC (see Figs. 2 and 4). This observation is because bent waveguides with straight lines can also bring the transverse coupling effect. Thus, after bent waveguides connect, the original coupling region length is longer. The splitting ratio can be unchanged if the coupling region length is reduced after using bent waveguides. In the same footprint, CGC coupler has better performance than X coupler.

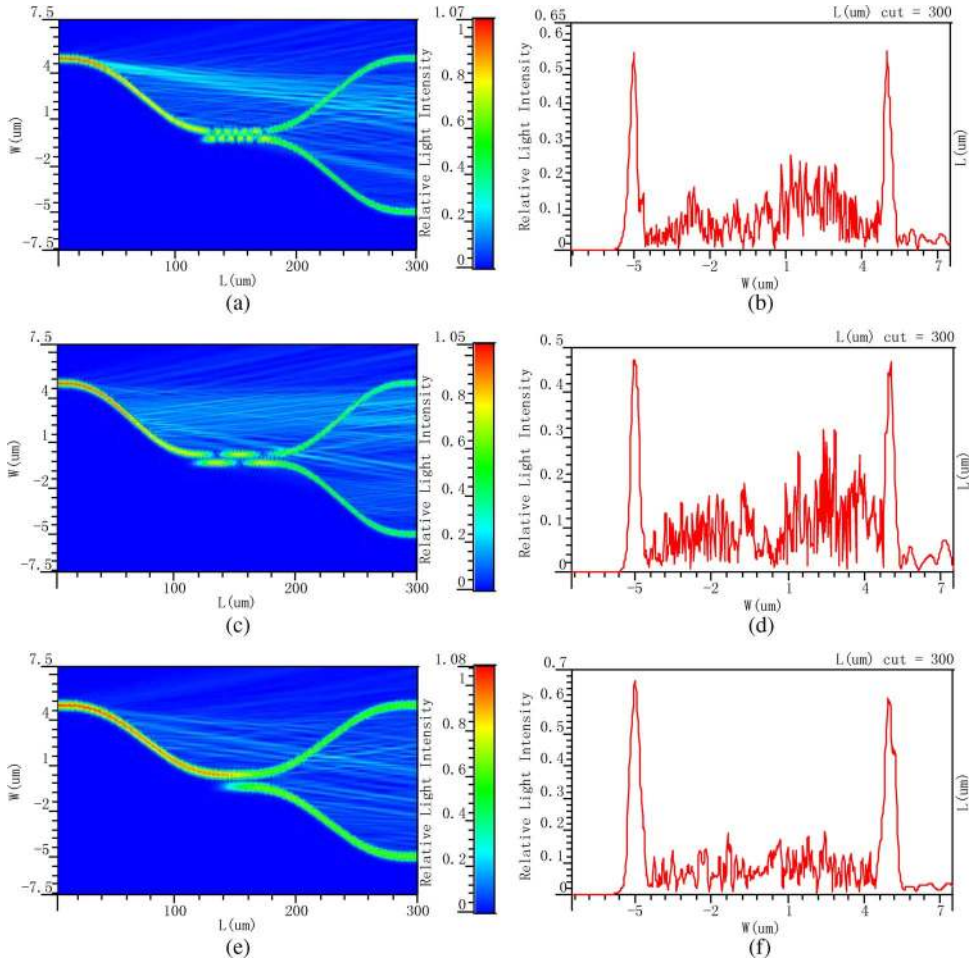

Fig. 2. Optical field of X coupler when (a) $w = 0.35$, $s = 0.05$; (c) $w = 0.35$, $s = 0.2$; and (e) $w = 0.55$, $s = 0.2$ μm. Output power of X coupler when (b) $w = 0.35$, $s = 0.05$; (d) $w = 0.35$, $s = 0.2$; and (f) $w = 0.55$, $s = 0.2$ μm.

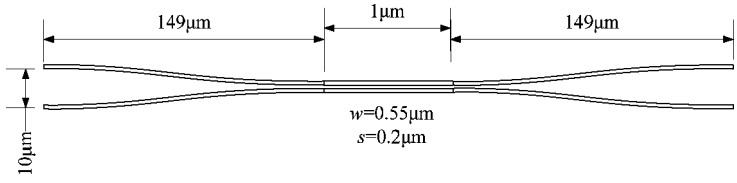

Fig. 3. Layout and detailed parameters of X coupler.

2.4. Design and Optimization of 2 × 2 MMI Coupler

The MMI coupler based on the self-imaging principle [14] has three kinds of interference mechanism, namely, general, paired, and symmetrical.

Paired interference is selected in the present paper. Input waveguides are set in the position $\pm w_e/6$ of the multimode waveguide

$$w_e = w + \frac{\lambda_0}{\pi} \cdot \left(\frac{n_c}{n_r}\right)^{2\sigma} \left(n_r^2 - n_c^2\right)^{-\frac{1}{2}} \tag{5}$$

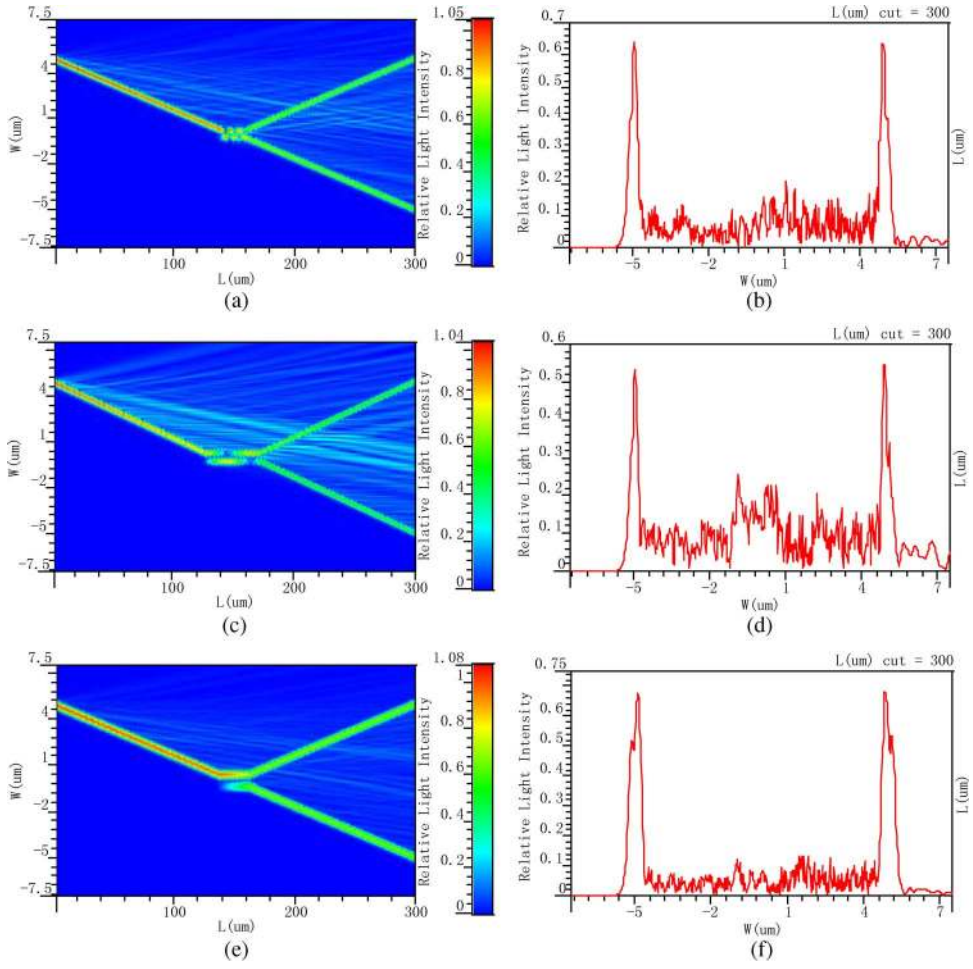

Fig. 4. Optical field of CGC when (a) $w = 0.35$, $s = 0.05$; (c) $w = 0.35$, $s = 0.2$; and (e) $w = 0.55$, $s = 0.2$ μm. Output power of CGC when (b) $w = 0.35$, $s = 0.05$; (d) $w = 0.35$, $s = 0.2$; and (f) $w = 0.55$, $s = 0.2$ μm.

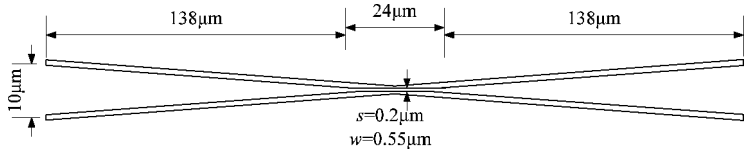

Fig. 5. Layout and detailed parameters of CGC.

where w is the multimode waveguide width, λ_0 is the center wavelength, $\sigma = 0$ is set for TE mode, $\sigma = 1$ is set for TM mode, n_c is the effective refractive index of cladding, and n_r is the effective refractive index of core.

The multimode waveguide length can be expressed as follows:

$$L_{MMI} = \frac{L_\pi}{2} = \frac{\pi}{2(\beta_0 - \beta_1)} \approx \frac{2nw_e^2}{3\lambda_0} \tag{6}$$

where L_π represents the coupling length of the two lowest-order modes. β_0 and β_1 are the propagation constants of the lateral mode 0 and mode 1, respectively.

TABLE 1

Comparison of CGC and X Coupler

Type of coupler	s (μm)	w (μm)	L (μm)	L_x (μm)	EL (dB)
CGC	0.05	0.35	141	18	0.85
CGC	0.2	0.35	127	46	1.2
X	0.05	0.35	142	16	1.4
X	0.2	0.35	128.5	43	0.96
CGC	0.2	0.55	138	24	0.6
X	0.2	0.55	149.5	1	0.73

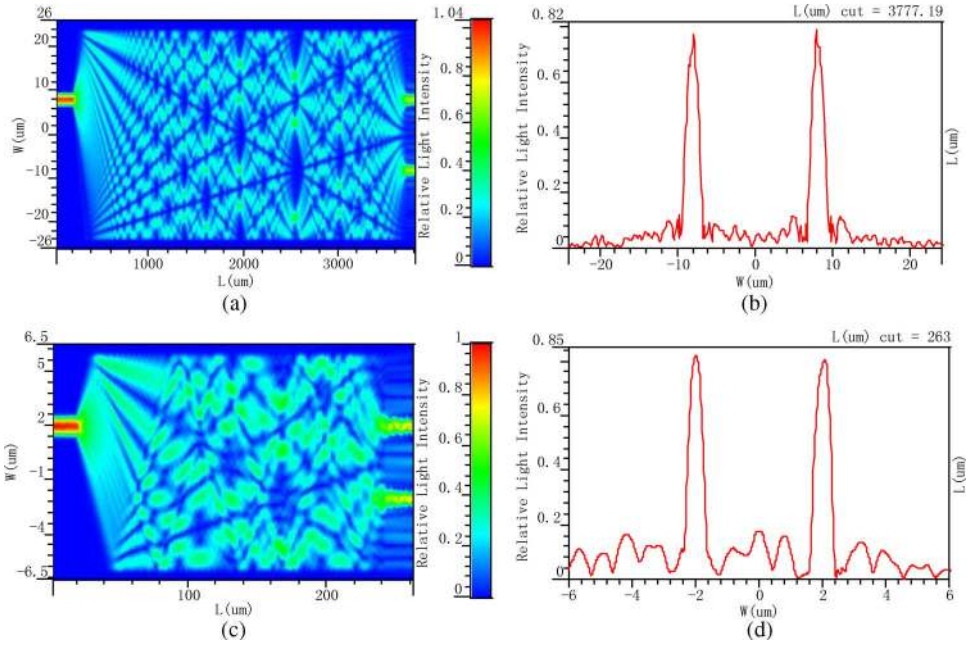

Fig. 6. Optical field of MMI coupler when $w =$ (a) 48 μm and (c) 12 μm. Output power of MMI coupler when $w =$ (b) 48 μm and (d) 12 μm.

According to (5), in the weak restrictive waveguide, we can obtain $n_c/n_r \approx 1$. In either TE or TM polarization mode, the obtained L_{MMI} values are approximately equal. Thus, MMI coupler has good polarization properties in the weak restrictive waveguide. However, in strong restrictive waveguide, e.g., $n_c = 1.45$, $n_r = 3.46$, $n_c/n_r = 0.419$, and $w = 6$ μm, we obtain that $L_{MMI} \approx 56.41$ μm in TE polarization mode and $L_{MMI} \approx 54.07$ μm in TM polarization mode according to (5) and (6). The L_{MMI} values in different polarization mode show relatively larger difference. Thus, the coupler has relatively poor polarization properties in strong restrictive waveguide.

In this paper, the coupler is simulated via BPM. The multimode waveguide width is expressed as w. The couplers with w of 48, 24, 15, 12, and 6 μm are simulated in this paper. Fig. 6 shows the optical field and output power of MMI coupler when $w = 48$ μm and 12 μm. A greater w value results in increased model numbers that can be stimulated, clearer image points, and less excess loss. However, this value also produces a larger device, as shown in Fig. 6. Therefore, the multimode waveguide width is gradually reduced from $w = 48$ μm to achieve a smaller 2×2 MMI coupler with good properties.

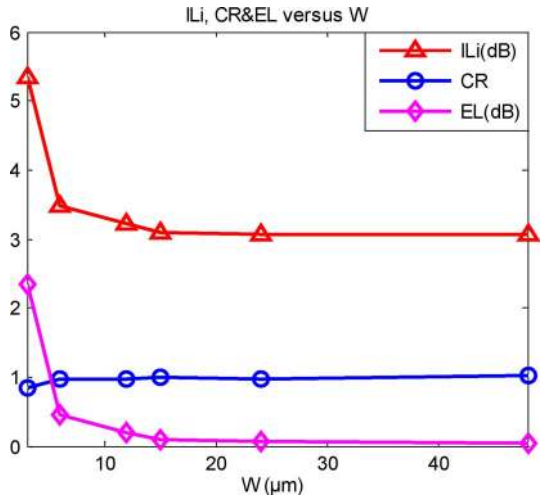

Fig. 7. Insert loss, excess loss, and splitting ratio versus w.

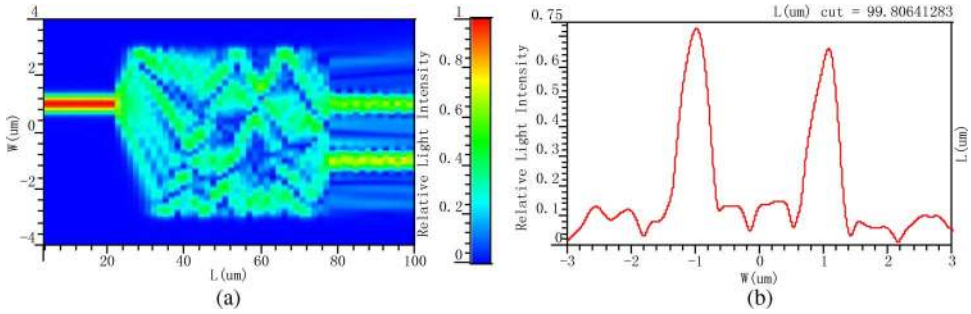

Fig. 8. (a) Optical field and (b) output power of MMI coupler with a linear input/output waveguide when $w = 6$ μm.

Fig. 7 shows how the multimode waveguide width affects insert loss, excess loss, and splitting ratio. The insertion and excess losses of the coupler increase with decreasing w when $w \leq 48$ μm. When 6 μm $\leq w \leq$ 48 μm during the simulation process, the change is not apparent. Reducing w from 6 μm to 3 μm results in increased excess loss, poor device uniformity, and vague image points.

Taking the device footprint and excess loss into account, $w = 6$ μm is eventually selected. When $w = 6$ μm, we can calculate L_{MMI} as 56.41 μm [(5) and (6)]. The image points are observed and analyzed during the simulation process to reduce excess loss and determine the best image points. $L_{MMI} = 57$ μm is eventually selected. The optical field and output power of MMI coupler with a linear input/output waveguide are shown in Fig. 8.

Input/output waveguides are designed as tapered waveguides during optimization process to make the image point clearer, improve splitting ratio, and reduce loss. Fig. 9 shows the optical field and output power of MMI coupler after optimization. Before optimization, the excess loss of the coupler is 1.09 dB, and the splitting ratio is 0.903. After optimization, the excess loss of the coupler is 0.46 dB, and the splitting ratio is 1.013.

The center light wavelength λ is changed to analyze the coupler performance. Fig. 10 shows how the center wavelength affects insert loss, excess loss, and splitting ratio. Within a spectral range of 1.49 μm to 1.59 μm, excess loss is less than 1.55 dB. The simulation results show that the designed coupler has a wide range of wavelength response.

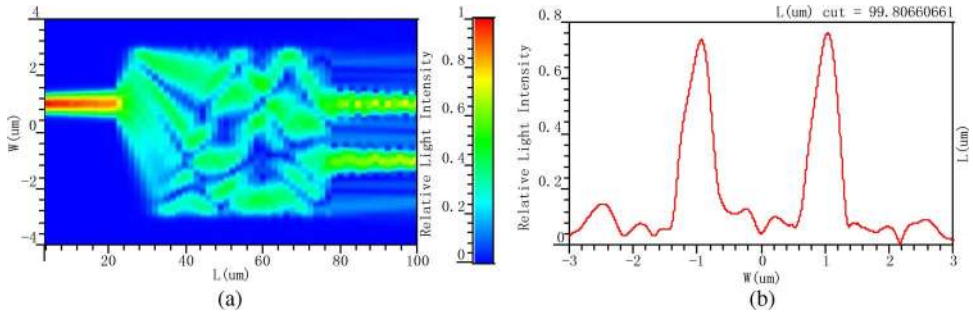

Fig. 9. (a) Optical field and (b) output power of MMI coupler with a tapered input/output waveguide when $w = 6$ μm.

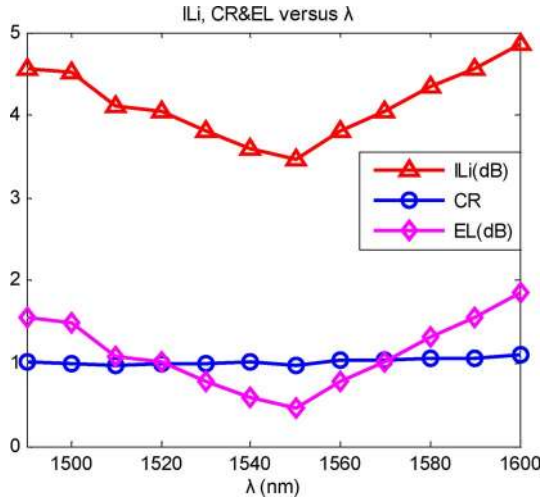

Fig. 10. Insert loss, splitting ratio, and excess loss versus λ.

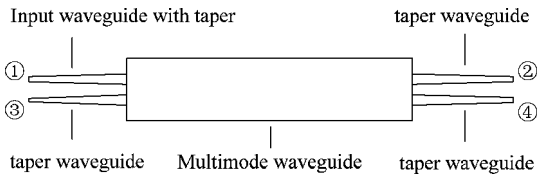

Fig. 11. Layout of the 2 $\times$ 2 MMI coupler when $w = 6$ μm.

Fig. 11 shows the layout of the designed 2 $\times$ 2 MMI coupler. The footprint of MMI regions is only 6 μm $\times$ 57 μm. The end of the input/output waveguides connected to the multimode waveguide is set to 1 μm. The other side of the waveguides numbered as 1, 2, and 4 are set to 0.65 μm, whereas 3 is set to 0.35 μm.

The designed MMI coupler in Fig. 11 can be applied directly to the microsystem. But we also need to test the coupler separately. The core diameter of single-mode fiber is between 4 μm and 10 μm, whereas the distance between the two output waveguides is only 2 μm. The coupler needs to be connected to the single-mode fiber using size spot converter, so the s-bend waveguide at the end of the output waveguides is used. The distance between output waveguides is set to 10 μm. Fig. 12 shows the optical field and output power of MMI coupler with s-bend waveguides.

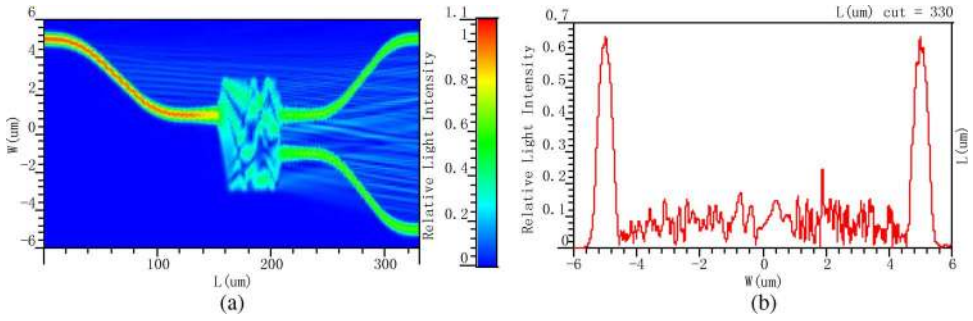

Fig. 12. (a) Optical field and (b) output power of MMI coupler with s-bend waveguides when $w = 6$ μm.

TABLE 2

Comparison of 2 × 2 Couplers

Coupler types	Materials	Footprint (μm×μm)	Splitting ratio	Excess loss (dB)	Wavelength response (μm)
X	SOI	10×300	48.82 : 51.18	0.79	1.545-1.555
CGC	SOI	10×300	50.21 : 49.79	0.6	1.545-1.555
MMI	SOI	6×100	50.66 : 49.34	0.46	1.49-1.59

3. Comparison of the Designed Couplers

As mentioned above, the couplers have better polarization properties in the weak restrictive waveguide than in strong restrictive waveguide. Moreover, the MMI coupler based on SOI have better polarization properties than X coupler and CGC. For MMI coupler, when $w = 6$ μm, we can calculate that L_{MMI} has a difference of 2.34 μm in TE and TM polarization modes, while the coupling region length of X coupler and CGC have a difference of more than 3 μm in TE and TM polarization mode.

The simulation results show that X coupler depends greatly on wavelength and has a large size. In the same footprint, CGC has relatively smaller loss and can be used as alternatives to X coupler. However, CGC also depends greatly on wavelength and is sensitive to polarization. MMI couplers have advantages such as compact construction, small size, simple fabrication techniques, large fabrication tolerance, low loss, and polarization insensitivity. Thus, MMI couplers are widely used in planar lightwave circuits. Table 2 shows a comparison of three kinds of couplers designed in this paper.

4. Conclusion

This paper has introduced the design of 2 × 2 coupler with silicon photonic nanowires for AWG demodulation integration microsystem. Three kinds of 2 × 2 couplers have been simulated through BPM. Compared with CGC and X coupler, MMI coupler has advantages of smaller footprint, lower loss, and wider bandwidth. During the simulation process, the best image points are found according to the self-imaging principle, and the input/output waveguides are optimized. The total footprint of the designed MMI coupler is 6 μm × 100 μm. The excess loss of the coupler after optimization can reduce to 0.46 dB, and the uniformity can reduce to 0.06 dB. The coupler has good properties within 1490 nm to 1590 nm. The designed coupler is highly compact and exhibits low excess loss, wide bandwidth, and good uniformity. The MMI coupler can meet the optoelectronic integration requirements.

References

[1] B. Jalali and S. J. Fathpour, "Silicon photonics," *J. Lightw. Technol.*, vol. 24, no. 12, pp. 4600–4615, Dec. 2006.

[2] H. Amir, S. Harish, K. David, Z. Yang, and C. Ray, "Optimum access waveguide width for 1× N multimode interference couplers on silicon nanomembrane," *Opt. Lett.*, vol. 17, no. 35, pp. 2864–2866, Sep. 2010.

[3] J. S. Rodgers, S. E. Ralph, and R. P. Kenan, "Self-guiding multimode interference threshold switch," *Opt. Lett.*, vol. 25, no. 23, pp. 1717–1719, Dec. 2000.

[4] Z. Le, S. Huang, J. Hu, M. Fu, and M. Zhang, "General self-imaging properties for line-tapered multimode interference couples," *Acta Optica Sinica*, vol. 31, no. 6, p. 0611003, 2011.

[5] F. Xu and A. W. Poon, "Silicon cross-connect filters using microring resonator coupled multimode-interference based waveguide crossings," *Opt. Lett.*, vol. 16, no. 12, pp. 8649–8657, Jun. 2008.

[6] S. S. Woo, C. S. Yeon, and J. N. Marie, "Integrated thin film InGaAsP laser and 1× 4 polymer multimode interference splitter on silicon," *Opt. Lett.*, vol. 32, no. 5, pp. 548–550, Mar. 2007.

[7] T. Amemiya, T. Shindo, D. Takahashi, S. Myoga, N. Nishiyama, and S. Arai, "Nonunity permeability in metamaterial-based GaInAsP/InP multimode interferometers," *Opt. Lett.*, vol. 36, no. 12, pp. 2327–2329, Jun. 2011.

[8] W. Chen, S. M. Eaton, H. Zhang, and P. R., "Broadband directional couplers fabricated in bulk glass with high repetition rate femtosecond laser pulses," *Opt. Lett.*, vol. 16, no. 15, pp. 11 470–11 480, Jul. 2008.

[9] D. Tanaka, Y. Ikuma, and H. Tsuda, "Comparative simulation of three types of 3-dB coupler using a Si wire waveguide," in *Proc. 3rd ICCE*, Aug. 2010, pp. 389–393.

[10] R. Halir, A. Maese-Novo, A. Ortega-Moñux, I. Molina-Fernández, J. G. Wangüemert-Pérez, P. Cheben, D.-X. Xu, J. H. Schmid, and S. Janz, "Colorless directional coupler with dispersion engineered sub-wavelength structure," *Opt. Lett.*, vol. 20, no. 12, pp. 13 470–13 477, Jun. 2012.

[11] K. Solehmainen, M. Kapulainen, M. Harjanne, and T. Aalto, "Adiabatic and multimode interference couplers on silicon-on-insulator," *IEEE Photon. Technol. Lett.*, vol. 18, no. 21, pp. 2287–2289, Nov. 2006.

[12] D.-X. Xu, S. Janz, and P. Cheben, "Design of polarization-insensitive ring resonators in silicon-on-insulator using MMI couplers and cladding stress engineering," *IEEE Photon. Technol. Lett.*, vol. 18, no. 2, pp. 343–345, Jan. 2006.

[13] J. Zhou, H. Shen, R. Jia, H. Liu, Y. Tang, C. Yang, C. Xue, and X. Liu, "Uneven splitting-ratio 1× 2 multimode interference splitters based on silicon wire waveguides," *Chin. Opt. Lett.*, vol. 9, no. 8, p. 082303, Aug. 2011.

[14] M. T. Hill, X. J. M. Leijtens, G. D. Khoe, and M. K. Smit, "Optimizing imbalance and loss in 2× 2 3-dB multimode interference couplers via access waveguide width," *J. Lightw. Technol.*, vol. 21, no. 10, pp. 2305–2313, Oct. 2003.

[15] L. C. Ozcan, F. Guay, R. Kashyap, and L. Martinu, "Fabrication of buried waveguides in planar silica films using a direct CW laser writing technique," *J. Non-Cryst. Solids*, vol. 354, no. 42-44, pp. 4833–4839, Nov. 2008.